MTV proteins unveil ER- and microtubule-associated compartments in the plant vacuolar trafficking pathway

María Otilia Delgadillo[a,1], Guillermo Ruano[a,1], Jan Zouhar[a,b], Michael Sauer[a,c], Jinbo Shen[d], Aleksandra Lazarova[a], Maite Sanmartín[a], Louis Tung Faat Lai[a,e], Cesi Deng[a,e], Pengwei Wang[f], Patrick J. Hussey[g], José Juan Sánchez-Serrano[a], Liwen Jiang[e], and Enrique Rojo[a,2]

[a]Centro Nacional de Biotecnología, Consejo Superior de Investigaciones Científicas, Cantoblanco, E-28049 Madrid, Spain; [b]Central European Institute of Technology, Mendel University in Brno, CZ-61300 Brno, Czech Republic; [c]Department of Plant Physiology, University of Potsdam, 14476 Potsdam, Germany; [d]State Key Laboratory of Subtropical Silviculture, Zhejiang A&F University, Hangzhou 311300, China; [e]School of Life Sciences, Centre for Cell and Developmental Biology and State Key Laboratory of Agrobiotechnology, The Chinese University of Hong Kong, Shatin, New Territories, Hong Kong, China; [f]Key Laboratory of Horticultural Plant Biology (Ministry of Education), College of Horticulture and Forestry Sciences, Huazhong Agricultural University, Wuhan 430070, China; and [g]Department of Biosciences, Durham University, Durham DH1 3LE, United Kingdom

Edited by Natasha V. Raikhel, Center for Plant Cell Biology, Riverside, CA, and approved March 17, 2020 (received for review November 11, 2019)

The factors and mechanisms involved in vacuolar transport in plants, and in particular those directing vesicles to their target endomembrane compartment, remain largely unknown. To identify components of the vacuolar trafficking machinery, we searched for *Arabidopsis modified transport to the vacuole* (*mtv*) mutants that abnormally secrete the synthetic vacuolar cargo VAC2. We report here on the identification of 17 *mtv* mutations, corresponding to mutant alleles of *MTV2/VSR4*, *MTV3/PTEN2A MTV7/EREL1*, *MTV8/ARFC1*, *MTV9/PUF2*, *MTV10/VPS3*, *MTV11/VPS15*, *MTV12/GRV2*, *MTV14/GFS10*, *MTV15/BET11*, *MTV16/VPS51*, *MTV17/VPS54*, and *MTV18/VSR1*. Eight of the MTV proteins localize at the interface between the *trans*-Golgi network (TGN) and the multivesicular bodies (MVBs), supporting that the trafficking step between these compartments is essential for segregating vacuolar proteins from those destined for secretion. Importantly, the GARP tethering complex subunits MTV16/VPS51 and MTV17/VPS54 were found at endoplasmic reticulum (ER)- and microtubule-associated compartments (EMACs). Moreover, MTV16/VPS51 interacts with the motor domain of kinesins, suggesting that, in addition to tethering vesicles, the GARP complex may regulate the motors that transport them. Our findings unveil a previously uncharacterized compartment of the plant vacuolar trafficking pathway and support a role for microtubules and kinesins in GARP-dependent transport of soluble vacuolar cargo in plants.

vacuoles | trafficking | microtubules

The endomembrane system in plants has unique properties and functions. One that stands out prominently is the presence of very large vacuoles, which occupy most of the cellular volume in the majority of vegetative cells from the adult plant (1). These large vacuoles store, buffer, and sequester compounds, while allowing for rapid and energetically cheap cell expansion, which is essential for exploring the surrounding media and attaining the necessary resources for autotrophic growth. It is thought that constraints of this unique cellular landscape, dominated by vacuoles, have led to other alterations in the organization of endomembrane compartments and in the trafficking between them (2). For instance, the endoplasmic reticulum (ER), Golgi, *trans*-Golgi network (TGN), and multivesicular bodies (MVBs) are highly dynamic in plant cells, which may be required to elude the large vacuoles and maintain effective trafficking between these compartments. Due to the importance of vacuoles in plant growth and adaption to the environment, the mechanisms of trafficking to this compartment have been intensively studied, particularly in *Arabidopsis thaliana*. Based on sensitivity to genetic or pharmacological disruption, four independent vacuolar pathways for transport of membrane proteins to the tonoplast have been described in this model plant (3–6). In contrast, it is unclear whether different soluble cargoes are transported through separate pathways to the vacuole (7–9) or through a single route (10). Moreover, the machinery performing the different transport steps in the vacuolar trafficking pathways remains for the most part uncharacterized and many controversial issues persist. Paramount among those controversies is which anterograde and retrograde routes are taken by vacuolar sorting receptors (VSRs) to perform their function of selecting and directing soluble cargo toward the vacuole (8, 11–14). VSRs are arguably the most studied vacuolar trafficking factors in plants, but it is still unsettled where they bind their cargo, where they sort the vacuolar cargo away from secreted proteins, where they release their cargo, and whether they are then recycled back for further rounds of cargo sorting, and in that case, to which compartment (15, 16). In yeast and animals, VSRs are recycled via retromer vesicles to the TGN (17, 18), where the retromer carriers are tethered by the evolutionarily

Significance

Vacuoles play crucial roles in plant growth and adaptation to the environment. However, the mechanisms responsible for transporting membranes and contents to plant vacuoles remain largely uncharacterized, and the pathways and compartments involved are not fully charted. We report on the characterization of 17 vacuolar trafficking mutants that define a set of 13 cellular factors involved in transport of soluble vacuolar proteins in *Arabidopsis thaliana*. We show that two of these factors, the GARP tethering complex subunits VPS51 and VPS54, reside in an ER- and microtubule-associated compartment (EMAC) and that VPS51 interacts with the motor domain of kinesins, revealing an unknown compartment of the vacuolar pathway and suggesting that microtubules and kinesins participate in vacuolar trafficking in plants.

Author contributions: J.Z., M. Sauer, L.J., and E.R. designed research; M.O.D., G.R., J.Z., M. Sauer, J.S., A.L., M. Sanmartín, L.T.F.L., C.D., and E.R. performed research; P.W. and P.J.H. contributed new reagents/analytic tools; J.J.S.-S. and E.R. analyzed data; and E.R. wrote the paper.

The authors declare no competing interest.

This article is a PNAS Direct Submission.

See online for related content such as Commentaries.

[1]M.O.D. and G.R. contributed equally to this work.

[2]To whom correspondence may be addressed. Email: erojo@cnb.csic.es.

This article contains supporting information online at https://www.pnas.org/lookup/suppl/doi:10.1073/pnas.1919820117/-/DCSupplemental.

First published April 22, 2020.

conserved GARP multisubunit tethering complex and by coiled-coil golgins (19–24). Evidence from mammalian cells indicates that retromer vesicles track along microtubules in their way from endosomes to the TGN (25), transported by the motor protein dynein (26). There is evidence that retromer vesicles may also recycle VSRs in plants (27), but a role for microtubules in vacuolar trafficking has not been documented in these organisms (28). Moreover, plant genomes do not encode dyneins. Compared to metazoan genomes, plants contain a much larger number of kinesins, which probably take over functions carried out by dynein in animals (29). However, most plant kinesins remain functionally uncharacterized and a link to vacuolar trafficking has not been reported yet for this family of motor proteins. To clarify how vacuolar trafficking is performed in plants and solve the standing controversies, it is crucial to identify the molecular components orchestrating the trafficking reactions in the different pathways.

We have devised a genetic screen to identify vacuolar trafficking factors in *Arabidopsis* by isolating *modified transport to the vacuole* (*mtv*) mutants affected in the transport of the synthetic vacuolar cargo VAC2 (30). The rationale of the screen is based on the observation that interference with vacuolar trafficking in *Arabidopsis* often leads to abnormal secretion of vacuolar proteins into the apoplast. In wild-type (WT) plants, VAC2 localizes to the vacuole, where it is inactive. In the apoplast, VAC2 inhibits the *WUSCHEL* signaling pathway and reduces the shoot apical meristem (SAM) size (30), so *mtv* mutants that secrete VAC2 are identified by their smaller, and even terminated SAMs (31–33). We have previously reported on the map-based cloning of *mtv1*, *mtv2*, and *mtv4*, which corresponded, respectively, to mutants alleles of an EPSIN N-terminal homology domain containing protein, of the vacuolar sorting receptor VSR4, and of the ARF GTPase-activating protein AGD5 (34, 35). Here, we report the cloning and characterization of 17 additional *mtv* mutants that define a set of 13 *MTV* genes whose activity is required for vacuolar transport of VAC2 and other soluble cargoes. The results presented here unveil a previously unknown compartment in the plant vacuolar trafficking pathway and support a role for microtubules and kinesins in GARP-dependent transport of soluble vacuolar cargo.

Results

Identification of *mtv* Mutants. To identify factors required for vacuolar trafficking in plants, we performed a large screen on an ethyl methanesulfonate (EMS)-mutagenized M_2 population expressing *VAC2*. We selected from independent pools 23 mutants with strong *mtv* phenotype for further characterization. The mutants displayed early termination of the SAM only in the presence of the VAC2 transgene (Fig. 1*A*). To identify the causative mutations in the selected set, we crossed the mutants, in Ler background, with Col-0 plants and obtained the corresponding F_2 mapping populations. We selected F_2 plants with strong *mtv* SAM termination phenotype for genotyping. Three of the mutations (*mtv3-1*, *mtv9-1*, and *mtv11-1*) were identified through classic map-based cloning using polymorphic PCR markers, whereas the remaining 20 mutations were analyzed through next-generation sequencing (NGS). The *mtv3-1* mutation

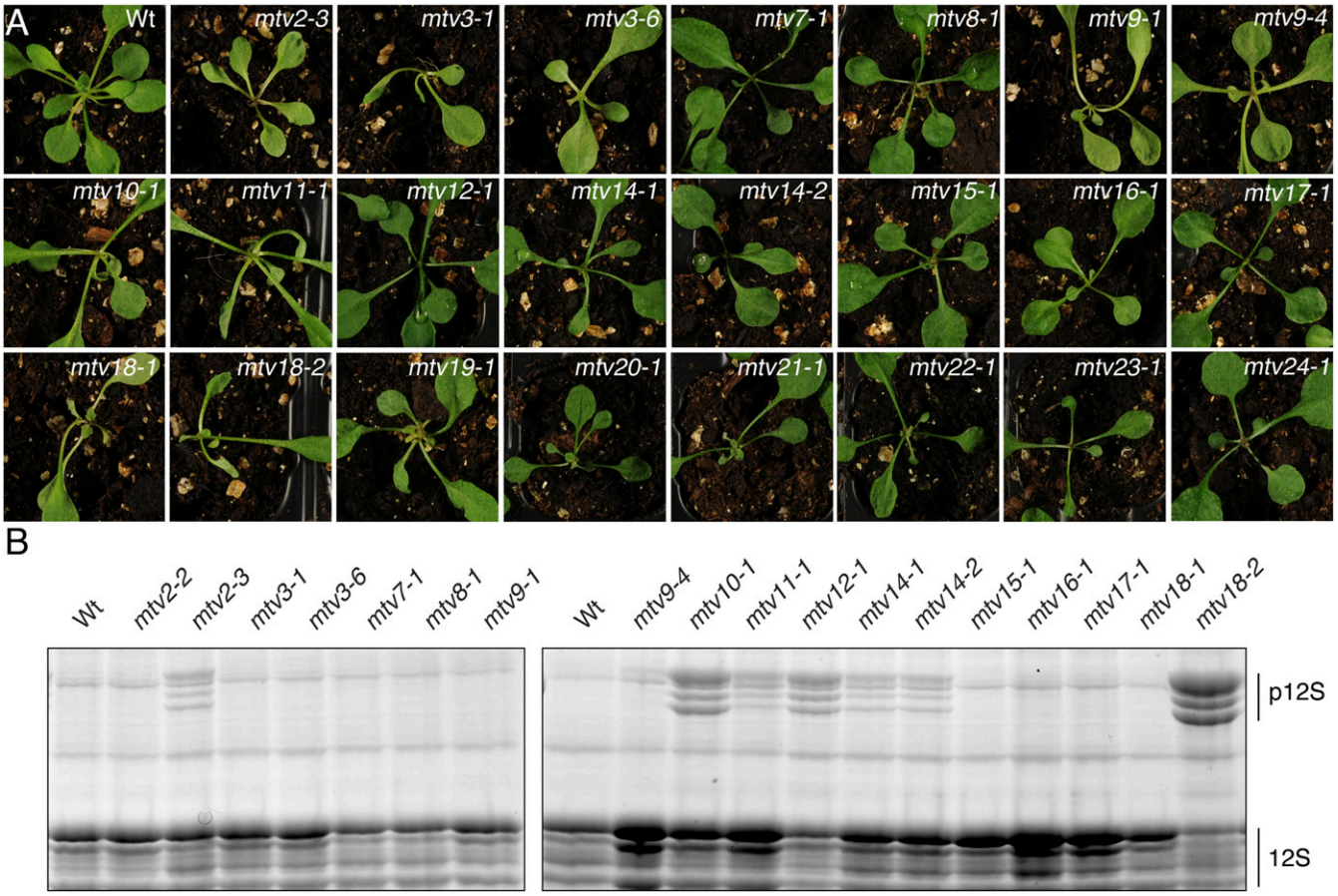

Fig. 1. *mtv* EMS-mutants show defects in vacuolar trafficking of VAC2 and 12S globulins. (*A*) SAM termination phenotype of the *mtv* mutants expressing *VAC2*. WT plants expressing VAC2 are shown for comparison. (*B*) Sodium dodecyl sulfate–polyacrylamide gel electrophoresis analysis of proteins extracted from mature seeds of the indicated genotypes. The position of processed (12S) and precursor forms of 12S (p12S) globulins are indicated.

was delimited to a region in the top of chromosome 3 containing 28 genes. We sequenced candidate genes in the region and found a missense mutation (G167R) in the At3g19340 gene that encodes PTEN2A, a phosphoinositide (PI) 3-phosphatase. The mutation affects a glycine residue that is conserved in all *PTEN* homologs from plants to animals, consistent with its relevance for protein function. Indeed, mutations in the corresponding glycine of human *PTEN*, a tumor suppressor gene, are frequently associated with cancer (36). Mapping of *mtv9-1* delimited a region on the top of chromosome 1 containing 34 genes. Sequencing of the genes in this region revealed a nonsense mutation (R51*) in the *At1g24560* gene, which had an unknown function at the time. However, *At1g24560*/*PUF2* was recently reported to encode a RAB5 effector involved in vacuolar transport (37). The *mtv11-1* mutation was mapped to a region in the bottom of chromosome 4 containing 80 genes. Through sequencing of candidate genes in that range, we identified a mutation disrupting a splice acceptor site in the seventh intron of the At4g29380 gene, encoding the VPS15 subunit of the sole PI 3-kinase (PI3K) present in plants. A knockout mutation in *VPS15* has been previously reported to cause pollen lethality in *Arabidopsis* (38), so we presumed that the *mtv11-1* allele should retain partial VPS15 activity. Analysis by RT-PCR revealed that most of the *At4g29280*/*VPS15* transcripts in *mtv11-1* plants retained the seventh intron (*SI Appendix*, Fig. S1 *A*–*C*), which causes a frameshift and a premature stop codon that eliminates most of the protein sequence. There were also significant amounts of transcripts that spliced out the seventh intron utilizing an alternative splice-acceptor site four nucleotides downstream of the original one, which also causes a frameshift and the deletion of most of the protein sequence. Importantly, we detected transcripts that spliced out of the eighth exon together with the seventh and the eighth introns (*SI Appendix*, Fig. S1*D*). This exon-skipping event produces transcripts that maintain the open reading frame and encode for a VPS15 protein lacking the central helical domain but retaining the N-terminal kinase domain and three of the four C-terminal WD repeats of the C-terminal WD40 domain, which could account for the partial activity of this allele.

Through NGS, we sequenced DNA from pools of 100 to 200 *mtv* plants of each of the remaining 20 mutants, using barcoding and a single Illumina lane and obtaining an estimated read depth of 26 to 30 reads per base and pooled mutant DNA. For each mutant, the region enriched in Ler polymorphisms was delimited (*SI Appendix*, Fig. S2) and the candidate variants in those regions considered. We identified, and confirmed through analyses of independent alleles (see below), the causative mutations of the *mtv* phenotype for 14 of the mutants (*SI Appendix*, Fig. S2). For the remaining six mutants, the causative mutations have yet to be confirmed and will be reported elsewhere. Among the 14 mutants identified, we found another allele of *MTV3*/*PTEN2A* and of *MTV9*/*PUF2*, as well as alleles of the vacuolar sorting receptors *VSR1* and *VSR4*, the Qc-SNARE *BET11*, the GARP tethering complex subunits *VPS51* and *VPS54*, the CORVET tethering complex subunit *VPS3*, the ARF GTPase *ARFC1*, the RAB5 effector *EREL1*, the RME-8 homolog *GRV2*/*KAM2*, and *GFS10*, a gene of unknown molecular function but previously linked to vacuolar trafficking (39). The nature of the mutations was as follows: 1) nonsense mutations in *VSR4* (*mtv2-3*/*vsr4-3*: Q222*), *ARFC1* (*mtv8-1*/*arfc1-1*: W8*), *VPS3* (*mtv10-1*/*vps3-1*: Q923*), *GRV2* (*mtv12-1*/*grv2-10*: W167*), *GFS10* (*mtv14-1*/*gfs10-3*: W38* and *mtv14-2*/*gfs10-4*: W158*), *BET11* (*mtv15-1*/*bet11-1*: R101*), *VPS54* (*mtv17-1*/*vps54-1*: W1014*), and *VSR1* (*mtv18-2*/*vsr1-8*: W234*); 2) missense mutation in *VSR1* (*mtv18-1*/*vsr1-7*: P259S); and 3) splice site mutations in *PTEN2A* (*mtv3-6*/*pten2a-6*: donor site third intron), *EREL1* (*mtv7-1*/*erel1-1*: acceptor site seventh intron), *PUF2* (*mtv9-4*/*puf2-4*: acceptor site fourth intron), and *VPS51* (*mtv16-1*/*vps51-1*: acceptor site seventh intron). Mutations in *MTV2*/*VSR4*, *MTV7*/*EREL1*, *MTV9*/*PUF2*, *MTV10*/*VPS3*, *MTV12*/*GRV2*/*KAM2*, *MTV14*/*GFS10*, *MTV16*/*VPS51*, and *MTV18*/*VSR* have been previously reported to affect vacuolar trafficking in *Arabidopsis* (13, 34, 37, 39–44). In contrast, there were no prior reports in plants of a role in vacuolar trafficking for *MTV3*/*PTEN2A*, *MTV8*/*ARFC1*, *MTV11*/*VPS15*, *MTV15*/*BET11*, and *MTV17*/*VPS54*. However, orthologs of MTV3/PTEN2A, MTV11/VPS15, and MTV17/VPS54 from yeast and mammals are involved in vacuolar trafficking in those organisms. Hence, most of the genes identified have been previously linked to vacuolar transport in some eukaryotic organism, highlighting the efficacy of the *mtv* screen for identifying vacuolar trafficking factors in plants.

Processing of 12S Globulins Is Altered in Several *mtv* Mutants. To test for possible alterations in trafficking of an endogenous vacuolar cargo, we analyzed the fate of 12S globulins, whose processing starts in MVBs and is completed in vacuoles (45). 12S globulin precursor forms accumulate when the vacuolar trafficking of these proteins is hindered (13). As shown in Fig. 1*B*, we observed significant levels of 12S globulin precursors in *mtv2-3*, *mtv10-1*, *mtv11-1*, *mtv12-1*, *mtv14-1*, *mtv14-2*, and *mtv18-2*, indicating that the corresponding mutations were disrupting vacuolar trafficking of these seed storage proteins. The defective trafficking of 12S globulins in the *mtv12-1*, *mtv14-1*, *mtv14-2*, and *mtv18-2* mutant alleles is consistent with previous reports of abnormal 12S globulin secretion in *MTV12*/*GRV2*, *MTV14*/*GFS10*/, and *MTV18*/*VSR1* mutants (13, 39, 40). In contrast, previously characterized *MTV2*/*VSR4* mutant alleles, including the null *vsr4-2* T-DNA allele, did not accumulate 12S globulins precursors due to redundancy from *VSR1* and *VSR3* (34). Thus, the presence of precursors in the *VSR4 mtv2-3* mutant implies that this allele dominantly interferes with *VSR1*/*VSR3* function. Conversely, the lack of accumulation of 12S globulin precursors in the *VSR1 mtv18-1* allele (Fig. 1*B*), suggests that the missense P259S mutation in this allele causes only a partial disruption of VSR1 function.

T-DNA Mutant Alleles of the Genes Identified Recapitulate the *mtv* Phenotype. To confirm that the mutations identified were causing the VAC2 and 12S globulin trafficking defects, we searched for T-DNA insertional alleles (*SI Appendix*, Fig. S3) and performed allelism tests. We crossed plants homozygous for the EMS alleles and the VAC2 transgene with heterozygous T-DNA insertional mutants in the corresponding candidate *MTV* genes. In the F_1 progeny from all of the crosses, we observed plants with the characteristic terminated SAM phenotype, which corresponded to the transheterozygotes containing the EMS and T-DNA alleles (*SI Appendix*, Fig. S4), whereas those plants that had the EMS and the WT alleles displayed normal indeterminate SAM growth phenotype, demonstrating that the EMS and T-DNA mutations were allelic. We then obtained in the next-generation homozygous T-DNA mutants for all of the alleles, except for the embryo lethal *vps3-2* allele of *MTV10*/*VPS3* and the gametophytic lethal *vps15-2* allele of *MTV11*/*VPS15*. All of the homozygous T-DNA mutants, including a weak *vps3-4* allele, displayed terminated SAMs, only in the presence of the VAC2 transgene (Fig. 2*A*), confirming that the corresponding genes were involved in VAC2 trafficking to the vacuole and that loss of their activities resulted in VAC2 secretion. The only exception was the *pten2a* T-DNA allele of *MTV3*/*PTEN2A*, which showed a slight reduction of SAM size but not termination, possibly due to the activity of the paralogous gene *PTEN2B*. Indeed, a double *pten2a pten2b* T-DNA mutant showed terminated SAMs in the presence of VAC2 (Fig. 2*A*). Furthermore, we obtained alternative evidence that the embryo-lethal *vps3-2* null mutant also had vacuolar trafficking defects. Light microscopy analysis revealed that the *vps3-2* null embryos had strong alterations in embryo patterning and cellular morphology, including enlarged intercellular spaces, absence of vacuoles in most cells, and the presence of

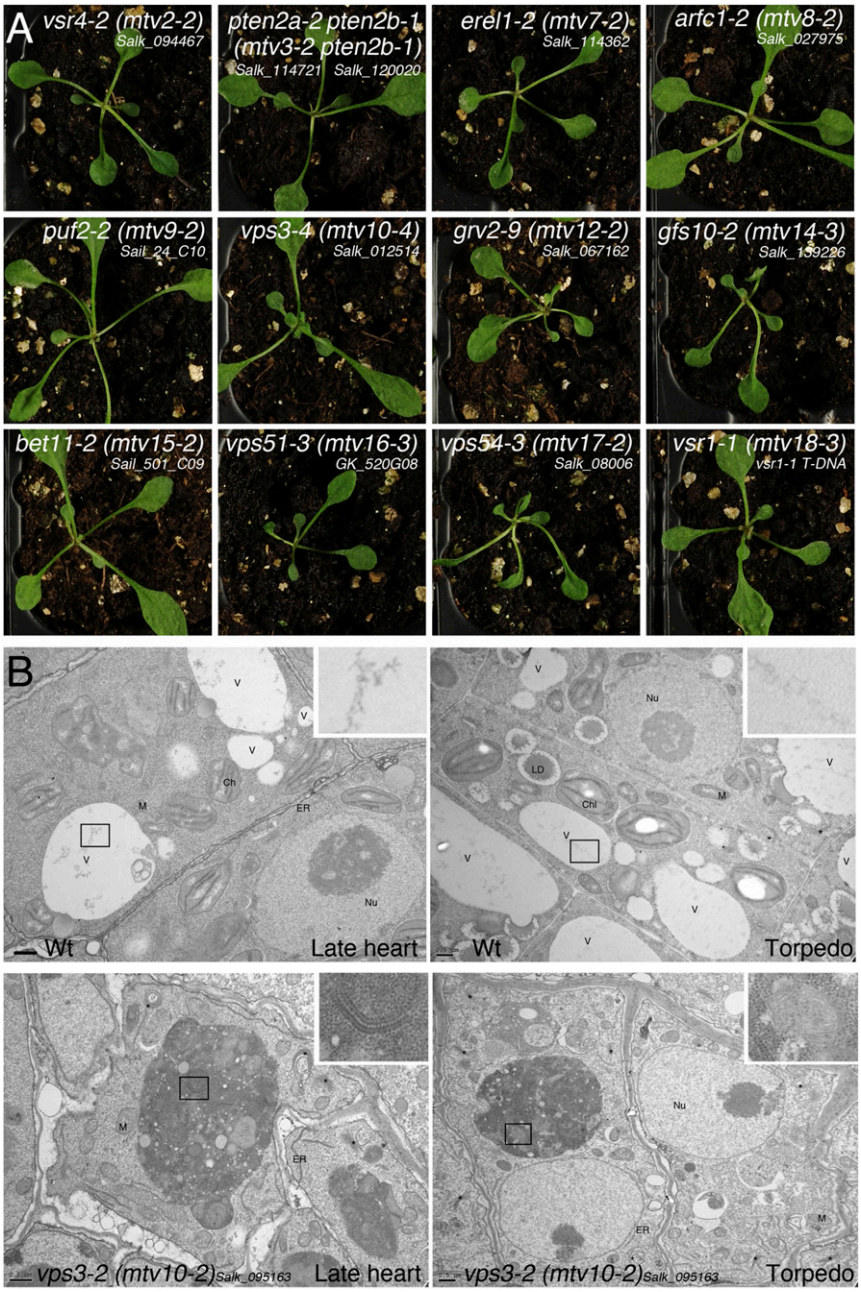

Fig. 2. Homozygous T-DNA mutants in *MTV* genes are defective in vacuolar trafficking. (*A*) SAM termination phenotype of homozygous T-DNA mutants expressing *VAC2*. (*B*) Transmission electron micrographs of embryos cells at the indicated developmental stages. The *vps3-2* (*mtv10-2*) embryos and the corresponding WT or heterozygous siblings (WT) from the same silique are shown. *Insets* are magnifications of the areas boxed in black, showing in *vps3-2* embryos ER (*Left Inset*) and mitochondria (*Right Inset*) inside the vacuole-like compartments. Asterisks, Golgi apparatus; Ch, chloroplast; ER, endoplasmic reticulum; LD, lipid droplet; M, mitochondria; V, vacuole. (Scale bars: 0.5 μm.)

unusual compartments intensely stained with toluidine blue (*SI Appendix*, Fig. S5*A*). Transmission electron microscopy confirmed that intercellular spaces in *vps3-2* embryos were highly expanded already at the heart stage (*SI Appendix*, Fig. S5*B*), suggesting that intracellular material is aberrantly secreted from early on during embryogenesis. At later stages, most *vps3-2* embryo cells lacked the usual vacuoles and instead accumulated vacuole-like compartments filled with electron-dense material and cytosolic organelles, including vesicles, ER, and mitochondria (Fig. 2*B*). We observed similar subcellular phenotypes in an independent *vps3-3* null allele. The aberrant compartments observed in *vps3* null embryos resembled those described in HeLa cells depleted of *VPS51*, which result from a block in transport of hydrolases to the lysosome/vacuole that impedes its lytic function (21). Altogether, phenotypic analysis of the T-DNA mutant alleles supports the role of the corresponding genes in vacuolar transport and corroborate that the EMS mutations identified are responsible for the defects in VAC2 trafficking.

Trafficking of Soluble Vacuolar Cargo Is Perturbed in *mtv* Seedlings. To further characterize vacuolar trafficking defects in the mutants, we analyzed the fate of fluorescently labeled soluble vacuolar markers that differ in the type of vacuolar sorting signals directing their transport to the vacuole: AALP-RFP (an RFP

fusion to AtAleurain) and CYSP-RFP (an RFP fusion to a cysteine protease), which contain sequence-specific vacuolar sorting signals with the canonical NPIR motif (46), and RFP-AFVY, which, like the VAC2 cargo, contains a C-terminal vacuolar sorting signal (47). When transiently expressed in cotyledon epidermal cells of WT plants, these fluorescent vacuolar markers uniformly labeled the cell interior, occupied almost entirely by the vacuole (Fig. 3). In contrast, we observed partial secretion of the vacuolar markers, with RFP labeling the cell contour, in all of the *mtv* mutants, except *grv2-5* and *bet11-2* (Fig. 3). The abnormal secretion of these vacuolar markers indicates that the corresponding *MTV* genes are involved in trafficking of cargoes with either sequence-specific or C-terminal vacuolar sorting signals. Moreover, although secretion of RFP-tagged vacuolar markers was not evident in the *grv2-5* and *bet11-2* plants, these two mutants did show alterations in the subcellular distribution of GFP-tagged vacuolar markers. In the *grv2-5* and *bet11-2* mutants, AALP-GFP and CYSP-GFP showed reduced vacuolar levels coupled to abnormal concentration at the lobes of epidermal cells, where mobile compartments could be observed (*SI Appendix*, Fig. S6 and Movies S1 and S2). The *grv2* mutant has previously been shown to accumulate clusters of endosomes (40), which is probably where AALP-GFP and CYSP-GFP are retained in their way to the vacuole. The *gfs10-2* mutant accumulated AALP-GFP and CYSP-GFP in large, mobile, and spherical endomembrane compartments, but in this case they were not concentrated in lobes at the cell periphery (*SI Appendix*, Fig. S6 and Movie S3). The mislocalization of fluorescent vacuolar markers observed in all of the mutants further substantiates that the *MTV* genes identified are required for proper transport of vacuolar cargo in *Arabidopsis*.

Most MTV Proteins Localize to the TGN–MVB Interface. The subcellular localization of four of the MTV proteins identified in this work, MTV2/VSR4, MTV7/EREL1, MTV12/GRV2, and MTV18/VSR1, had been previously reported. Immunoelectron microscopy studies had shown that endogenous VSRs reside primarily at the Golgi, TGN, and MVBs (45, 48), while fluorescence microscopy studies indicated that MTV7/EREL1 and MTV12/GRV2 localize to MVBs (41, 43). To examine the subcellular localization of the remaining MTV proteins, we expressed fluorescently tagged versions in *Nicotiana benthamiana* cells under the *UBIQUITIN10* promoter, which drives moderate levels of expression (49), and checked for colocalization

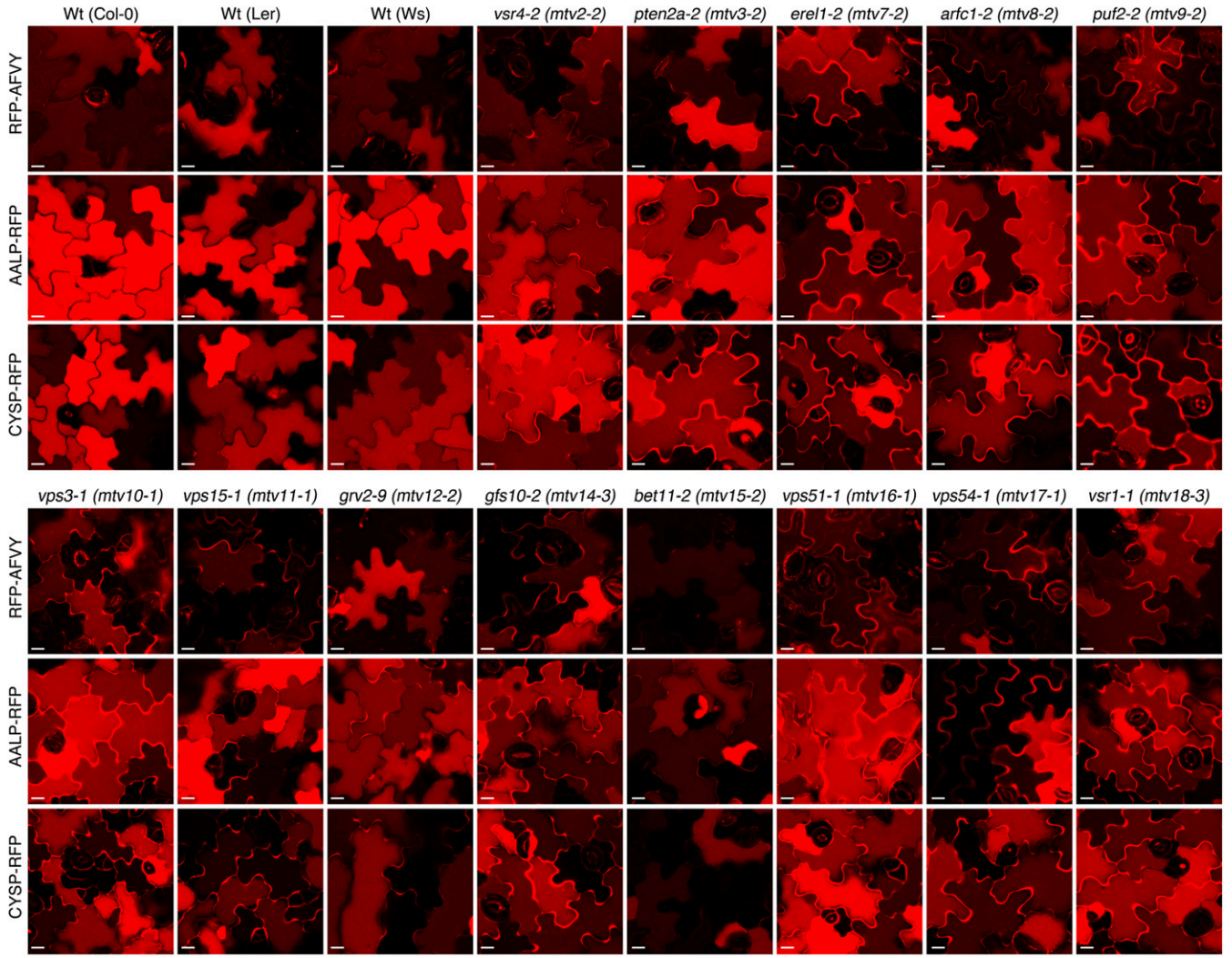

Fig. 3. Trafficking of cargo with different types of vacuolar sorting signals is perturbed in *mtv* mutants. Single confocal images of cotyledon cells from *Arabidopsis* seedlings of the indicated mutant genotypes or of the corresponding WT backgrounds (Ws for the vsr1-1 T-DNA allele, Col-0 for the rest of the T-DNA alleles, and Ler for EMS alleles) transiently transformed with RFP-AFVY, AALP-RFP, and CYSP-RFP. (Scale bars: 10 μm.)

with established organelle markers. MTV9/PUF2 and MTV10/VPS3 fused to RFP colocalized with the MVB marker YFP-ARA7 but not with the *cis*-Golgi marker YFP-MEMB12 or the TGN marker YFP-VTI12 (*SI Appendix*, Figs. S7 and S8), which agrees with the localization recently observed in *Arabidopsis* root cells (37, 44). We noted that MVBs labeled with RFP-PUF2 or RFP-VPS3 were abnormally enlarged, raising questions about the significance of this localization. Importantly, a *35S:GFP-VPS3* construct, which colocalizes with RFP-VPS3 in the enlarged MVBs in *Nicotiana* (*SI Appendix*, Fig. S9), does not cause MVB enlargement when expressed transiently in *Arabidopsis* cotyledons, and furthermore, it complements the ALEU-RFP trafficking defects of the *vps3-1* mutant (*SI Appendix*, Fig. S9), supporting that VPS3 is a bona fide MVB associated protein. In contrast, *35S:GFP-MTV9*, which *in Nicotiana* colocalizes with RFP-MTV9 in the enlarged MVBs (*SI Appendix*, Fig. S9), also caused MVB enlargement when expressed transiently in *Arabidopsis* (*SI Appendix*, Figs. S10 and S11), and failed to complement the ALEU-RFP trafficking defects of the *puf2-2* mutant (*SI Appendix*, Fig. S10). In fact, overexpression of *35S:GFP-MTV9* in *Arabidopsis* WT protoplasts interfered with transport of the tonoplast marker RFP-VIT1, which was retained in the enlarged MVBs. This dominant-negative effect was specific for vacuolar trafficking, because the transport of the plasma membrane marker RFP-SCAMP was not affected (*SI Appendix*, Fig. S11). Although we cannot conclude from these results that the MVB is where PUF2 performs its endogenous function, its functional interaction with MVB-localized RAB5 proteins supports this notion (37). MTV8/ARFC1-RFP colocalized with the *trans*-Golgi marker STtmd-GFP and was separate from TGN and MVB markers (*SI Appendix*, Fig. S12). Moreover, *35S:ARFC1-GFP*, which colocalizes with ARFC1-RFP (*SI Appendix*, Fig. S9), complemented the defect in ALEU-RFP trafficking of the *arfc1-2* mutant (*SI Appendix*, Fig. S10). These results support that ARFC1 localizes at the *trans* side of the Golgi stack in plants, which differs from the TGN localization of its metazoan homolog ARL5 (50). MTV14/GFS10 is a multispanning membrane protein belonging to the OSCA family of mechanosensitive ion channels (51). In contrast to other members of the OSCA gene family, which localize to the plasma membrane (52, 53), GFS10 fused to GFP localized to intracellular compartments in *Nicotiana benthamiana* cells, albeit the N-terminal and C-terminal fusions displayed a different localization. A GFS10 N-terminal GFP fusion (GFP-GFS10) localized at the ER (*SI Appendix*, Fig. S13), whereas a C-terminal GFP fusion (GFS10-GFP) was found in amorphous structures and partially colocalizing with an MVB marker (*SI Appendix*, Fig. S14). However, we could not detect complementation of ALEU-RFP trafficking defects in the *gfs10-2* by transient expression of either of the constructs (*SI Appendix*, Fig. S10), so we cannot conclude which localization may correspond to that of the endogenous GFS10. However, the fact that both constructs were found in endomembrane compartments, rather than at the plasma membrane like other OSCA proteins, is consistent with the role of GFS10 in vacuolar trafficking. MTV15/BET11 fused to GFP colocalized with TGN and MVB markers, but not with Golgi markers (*SI Appendix*, Fig. S15). This localization also differs from the localization of the yeast and mammalian homolog Bet1, which is found in COPII vesicles and at the ER/Golgi interface (54, 55). *Arabidopsis* contains two Bet1-like paralogues, MTV15/BET11 and BET12. BET12 localizes to the Golgi (56) and is probably the ortholog of Bet1, while MTV15/BET12 may have acquired plant-specific functions at the TGN and MVBs. MTV3/PTEN2A-GFP showed a cytosolic distribution in *Nicotiana benthamiana* cells. We reasoned that lack of association with membranes could be due to failure to interact with cognate protein partners, so we expressed it stably in *Arabidopsis* under the control of its native promoter, to retain the expression and regulation of the endogenous gene. In *Arabidopsis* root cells, *pPTEN2A:PTEN2A-GFP* was found at the cytosol but also in punctate compartments that colocalized with the TGN marker VHA-a1-RFP and were separate from the Golgi marker YFP-MEMB12 and the MVB marker YFP-ARA7 (*SI Appendix*, Fig. S16). Interestingly, a GFP fusion of the protein encoded by the *mtv3-1* missense allele driven by the native promoter (*pPTEN2A:pten2aG167R-GFP*) showed reduced association with the TGN (*SI Appendix*, Fig. S16), indicating that the substitution of the conserved glycine interferes with the recruitment to membranes and that this is likely responsible for the defects in vacuolar trafficking observed in the *mtv3-1* mutant.

Overall, 11 of the 16 MTV proteins that we have characterized until now (this work and refs. 31 and 33–35) localize to the TGN–MVB interface. This implies that interfering with trafficking factors operating between these two compartments often leads to secretion of vacuolar proteins, supporting that transport from the TGN to the MVB is not a default process and requires active segregation of vacuolar proteins from those destined for secretion.

MTV16/VPS51 Interacts with MTV17/VPS54 and Recruits It to Endomembrane Compartments. *MTV16* and *MTV17* encode, respectively, the putative *Arabidopsis* orthologs of the VPS51 and VPS54 subunits of the GARP tethering complex. Interaction between *Arabidopsis* MTV16/VPS51 and MTV17/VPS54 has not been reported, but there is evidence for their interaction with the other subunits of the GARP complex, POK/VPS52 and HIT1/VPS53 (42, 57). There are also previous data on the localization of some of these proteins in plants, but the results are inconclusive. In tobacco, VPS51 fused to GFP was found in small punctate compartments, which showed limited colocalization with markers from the Golgi, the TGN, and the MVB (42). VPS52 was reported to colocalize with Golgi markers in onion cells (58), but in maize cells there was only minor colocalization with Golgi and MVB markers (59). To clarify where the GARP complex resides in plants, we analyzed N-terminal and C-terminal fusions to VPS51 and VPS54. C-terminal GFP fusions to VPS51 and VPS54 (VPS51-GFP and VPS54-GFP) labeled punctate structures in *Nicotiana benthamiana* cells (Fig. 4*A* and *SI Appendix*, Figs. S9 and S17), supporting that they associate with endomembrane compartments. These chimeric fusion proteins complement the ALEU-RFP trafficking defects of the corresponding mutants (*SI Appendix*, Fig. S10), indicating that their localization mirrors that of the endogenous proteins. Moreover, VPS51-GFP and VPS54-GFP colocalized with RFP-VPS51 in the punctate structures (Fig. 4*A* and *SI Appendix*, Fig. S9), indicating that the proteins reside on the same compartment. In fact, epitope-tagged VPS51 and VPS54 coimmunoprecipitate from detergent-solubilized protein extracts, supporting that the proteins interact physically in vivo (Fig. 4*B*). In agreement with this, N-terminal fluorescently tagged versions of VPS54 (GFP-VPS54 or RFP-VPS54), which are cytosolic when expressed alone, were recruited to punctate compartments when coexpressed with RFP-VPS51 or VPS51-GFP (Fig. 4 *C* and *D*). These results support that MTV16/VPS51 and MTV17/VPS54 are interacting subunits of a GARP complex associated with endomembrane compartments.

The GARP Complex Localizes to ER- and Microtubule-Associated Compartments. To identify the compartment where the GARP complex resides, we coexpressed RFP-VPS51, VPS51-GFP, and VPS54-GFP with the battery of endomembrane markers. Surprisingly, RFP-VPS51 did not colocalize with markers from the Golgi, the TGN, or the MVB (Fig. 5 *A*–*D*). Likewise, there was no colocalization of VPS51-GFP and VPS54-GFP with markers from these endomembrane compartments (*SI Appendix*, Fig. S17). To gain further evidence for this, we treated *Nicotiana* plants with brefeldin A (BFA) and wortmannin, which affect Golgi, TGN, and MVB structure and distribution. As expected,

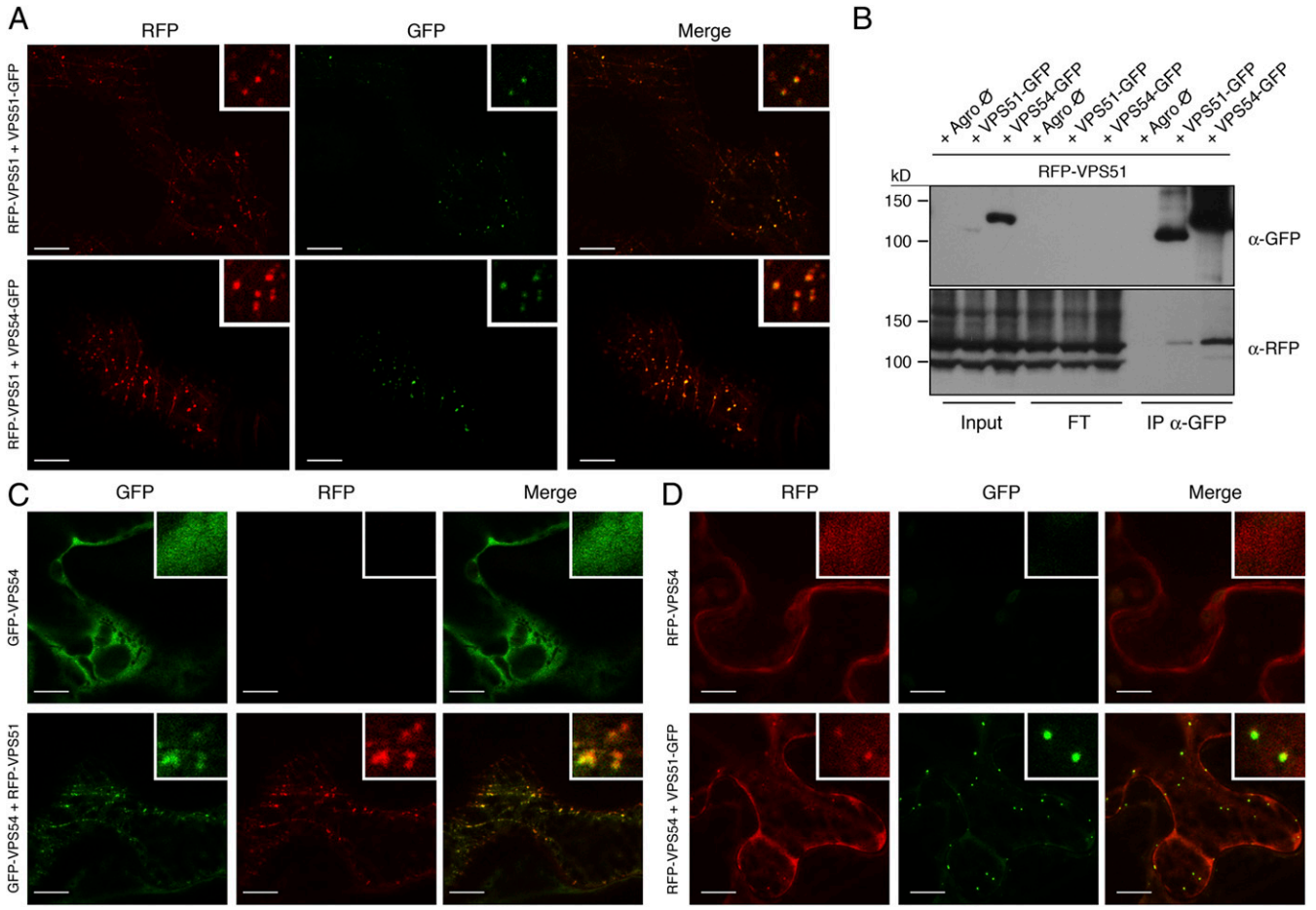

Fig. 4. VPS51 interacts with VPS54 and recruits it to endomembrane compartments. (*A*) Single confocal images of *Nicotiana benthamiana* epidermal cells cotransformed with *pUBI:RFP-VPS51* and *pUBI:VPS51-GFP* or *pUBI:VPS54-GFP*. (Scale bars: 10 μm.) (*B*) Coimmunoprecipitation assay of detergent-solubilized protein extracts with GFP-TRAP agarose beads. Extracts were from *Nicotiana benthamiana* leaves cotransformed with a *pUBI:RFP-VPS51* agrobacterium strain and agrobacterium without (+Agro Ø) or with the *pUBI:VPS51-GFP* (+VPS51-GFP) or *pUBI:VPS54-GFP* (+VPS54-GFP) plasmids. Western blots were incubated with anti-GFP (α-GFP) and anti-RFP (α-RFP) antibodies. The input, flowthrough (FT), and immunoprecipitated (IP α-GFP) fractions were analyzed. (*C*) Single confocal images of *Nicotiana benthamiana* epidermal cells expressing *pUBI:GFP-VPS54* alone (*Upper*) or together with *pUBI:RFP-VPS51*. (Scale bars: 10 μm.) (*D*) Max intensity projection of serial confocal images (depth: 4 μm) of *Nicotiana benthamiana* epidermal cells cotransformed with *pUBI:VPS51-GFP*, *pUBI:RFP-VPS54*, or both constructs together. (Scale bars: 10 μm.)

we observed resorption of the Golgi marker YFP-MEMB12 into the ER in BFA-treated plants and swelled MVBs labeled with YFP-ARA7 in wortmannin-treated plants, confirming that the drug treatments were effective. However, no changes in the distribution or morphology of GARP compartments were observed with these treatments (*SI Appendix*, Fig. S18), supporting that, in plants, the GARP complex resides in an endomembrane compartment distinct from the Golgi, the TGN, and the MVB. A hint to characterize the GARP-containing compartment was the very distinctive "beads-on-a-string" pattern shown by RFP-VPS51 (Figs. 4–6), which suggested a link to the cytoskeleton. A similar beads-on-a-string distribution had been previously described for a family of plant-specific proteins, the NETWORKED (NET) actin-binding proteins (60, 61). NET3C localizes to ER–plasma membrane contact sites (EPCS), where it interacts with VAP27 (62). RFP-VPS51 did not colocalize with GFP-NET3C or VAP27-YFP (Fig. 5 *E* and *F*), indicating that it is not present in EPCS. NET3B, which has a weaker actin binding capability than other members of the NET family, is distributed in punctate compartments associated with the ER and also labels the filamentous actin network (63). We detected colocalization of RFP-VPS51 with the punctate signal of NET3B-GFP but not with the filamentous signal (Fig. 5*G*), suggesting that the GFS10-labeled compartments may be connected to the ER. Indeed, the RFP-VPS51 signal was found always adjacent to the luminal ER marker GFP-HDEL (Fig. 5*H*), supporting that VPS51 localizes to a membrane compartment closely associated with the ER. Interestingly, the PI3K subunit MTV11/VPS15-GFP was also found associated to RFP-VPS51–labeled compartments (Fig. 5*I*), suggesting that their membranes may be enriched in 3-phosphorylated PIs. To directly test for a link of the GARP-containing compartments with the cytoskeleton, we coexpressed the fluorescently tagged VPS51 and VPS54 subunits together with actin or microtubule markers. Remarkably, the majority of the RFP-VPS51–labeled compartments aligned closely with microtubules labeled with GFP-MAP4, a fusion of GFP to the microtubule binding domain of the mammalian microtubule-associated protein 4 (Fig. 5*K*), but not with actin filaments labeled with GFP-Lifeact, a fusion of GFP to the first 17 aa of the yeast actin binding protein Abp140 (Fig. 5*J*). Similarly, VPS51-GFP and VPS54-GFP were also found linked to microtubules marked with KMD-RFP, a fusion of RFP to the motor domain (first 400 aa) of *Nicotiana benthamiana* kinesin NtKIN-7K (*SI Appendix*, Fig. S17 *E* and *J*). Together, these results show that the GARP-complex resides in ER- and microtubule-associated compartments (EMACs), which may have a distinctive PI composition. It has been previously

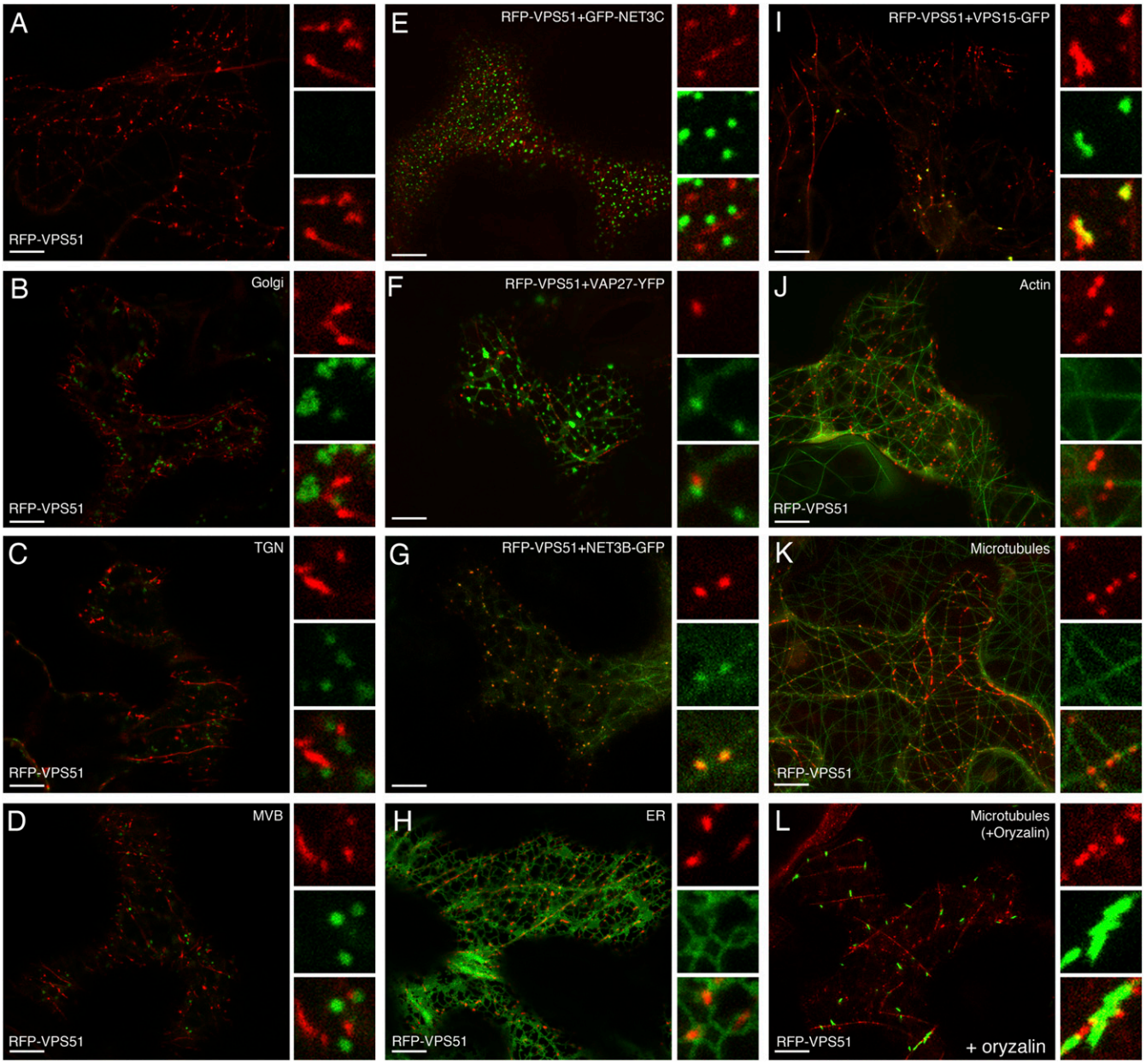

Fig. 5. VPS51 localizes to EMACs separate from Golgi, TGN, and MVB markers. (*A*) Max intensity projection of serial confocal images (depth: 6 μm) of *Nicotiana benthamiana* epidermal cells transformed with *pUBI:RFP-VPS51*. (*B–G*) Single confocal images of *Nicotiana benthamiana* epidermal cells cotransformed with *pUBI:RFP-VPS51* and the Golgi marker YFP-MEMB12 (*B*), the TGN marker YFP-VTI12 (*C*), the MVB marker YFP-ARA7 (*D*), the ERCS markers GFP-NET3C (*E*) and VAP27-YFP (*F*), and the ER-actin adaptor NET3B-GFP (*G*). (*H*) Max intensity projection of serial confocal images (depth: 4 μm) of *Nicotiana benthamiana* epidermal cells cotransformed with *pUBI:RFP-VPS51* and an ER marker GFP-HDEL. (*I*) Max intensity projection of serial confocal images (depth: 4 μm) of *Nicotiana benthamiana* epidermal cells transformed with *pUBI:RFP-VPS51* and *pUBI:VPS15-GFP*. (*J* and *K*) Max intensity projection of serial confocal images (depth: 10 μm) of *Nicotiana benthamiana* epidermal cells cotransformed with *pUBI:RFP-VPS51* and an actin cytoskeleton marker GFP-Lifeact (*J*) or the microtubule marker GFP-MAP4 (*K*). (*L*) Max intensity projection of serial confocal images (depth: 4 μm) of *Nicotiana benthamiana* epidermal cells cotransformed with *pUBI:RFP-VPS51* and GFP-MAP4 and treated for 6 h with 100 μM oryzalin. A merged image of the RFP (red pseudocolor) and GFP/YFP (green pseudocolor) signals is shown on the large panels. The small panels on the *Right* show a magnified detail, with the RFP and GFP/YFP signals separated and merged. (Scale bars: 10 μm.)

reported that ER junctions associated with microtubules are relatively immobile sites within the cell that are maintained even after microtubule destabilization (64). Time-lapse imaging revealed that a significant fraction of EMACs remained stationary (Movies S4–S9), which is concordant with the stability reported for ER junctions associated with microtubules, but exceptional for endomembrane compartments in plants. We then tested whether the distinctive distribution of EMACs requires intact microtubules, by treating plants with oryzalin. As expected, oryzalin caused destabilization of the microtubule filaments and their aggregation into small segments that probably correspond to bundled microtubule fragments (Fig. 5*L*). Importantly, oryzalin treatment did not disrupt the RFP-VPS51 beads-on-a-string pattern (Fig. 5*L*), suggesting that this arrangement is stable even when the microtubule scaffold is disassembled. Moreover, the fragmented microtubule bundles in

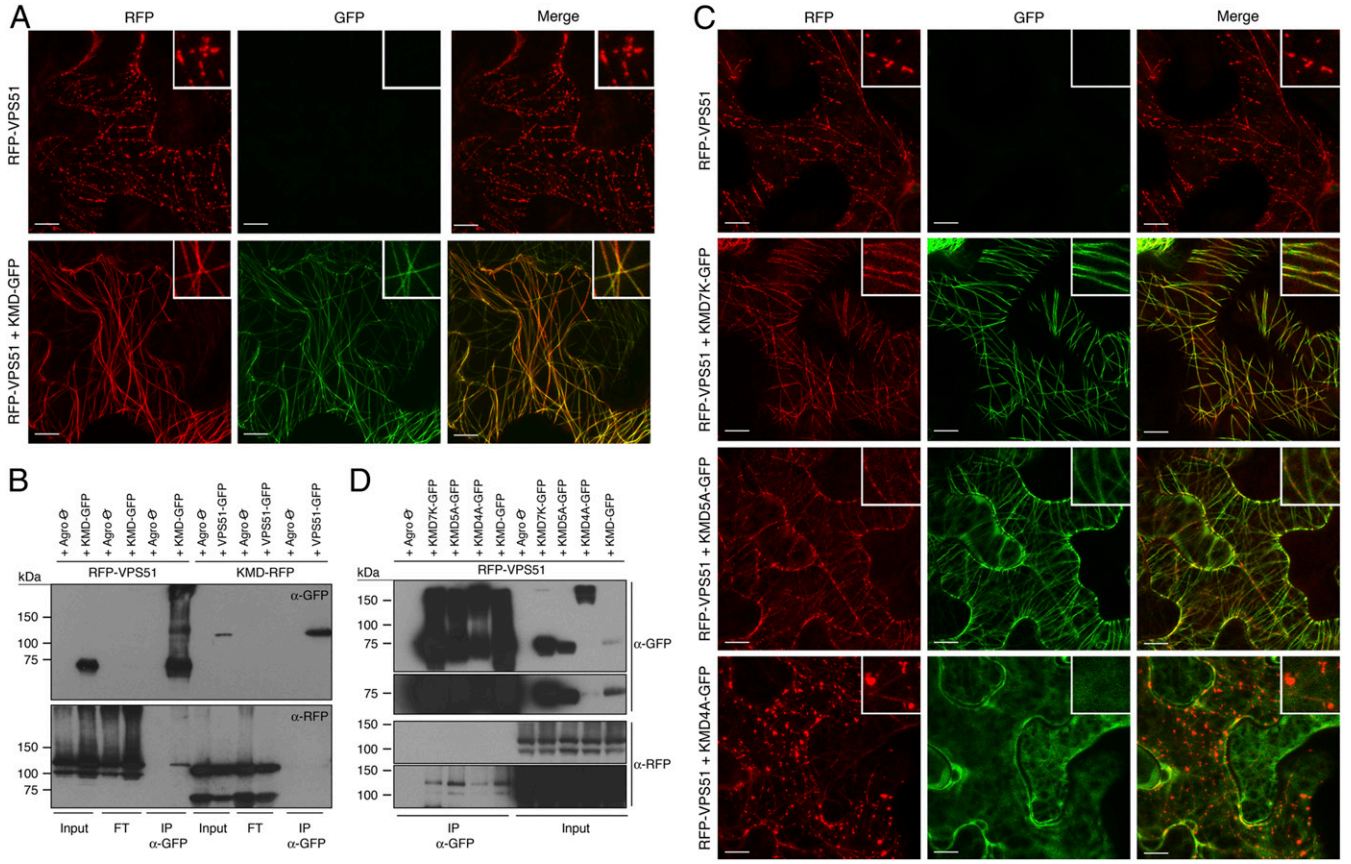

Fig. 6. VPS51 interacts with the motor domain of kinesins. (*A*) Max intensity projection of serial confocal images of *Nicotiana benthamiana* epidermal cells transformed with *pUBI:RFP-VPS51* (depth: 8 μm) or cotransformed with *pUBI:RFP-VPS51* and *35S:KMD-GFP* (depth: 10 μm). (Scale bars: 10 μm.) (*B*) Coimmunoprecipitation assay of detergent-solubilized protein extracts with GFP-TRAP agarose beads. Extracts were from *Nicotiana benthamiana* leaves cotransformed with the *pUBI:RFP-VPS51* agrobacterium strain and agrobacterium without (+Agro Ø) or with the *35S:KMD-GFP* plasmid (+KMD-GFP), or cotransformed with the *35S:KMD-RFP* agrobacterium strain and agrobacterium without (+Agro Ø) or with the *35S:VPS51-GFP* plasmid (+VPS51-GFP). Western blots were incubated with anti-GFP (α-GFP) and anti-RFP (α-RFP) antibodies. The input, flowthrough (FT), and immunoprecipitated (IP α-GFP) fractions were analyzed. (*C*) Max intensity projection of serial confocal images of *Nicotiana benthamiana* epidermal cells transformed with *pUBI:RFP-VPS51* (depth: 6 μm) or cotransformed with *pUBI:RFP-VPS51* and *35S:KMD7K-GFP* (depth: 4 μm), *35S:KMD5A-GFP* (depth: 4 μm), or *35S:KMD4A-GFP* (depth: 4 μm). (Scale bars: 10 μm.) (*D*) Coimmunoprecipitation assay of detergent-solubilized protein extracts from *Nicotiana benthamiana* leaves cotransformed with the *pUBI:RFP-VPS51* agrobacterium strain and agrobacterium without (+Agro Ø) or with the *35S:KMD7K-GFP* (+KMD7K-GFP), *35S:KMD5A-GFP* (+KMD5A-GFP), *35S:KMD4A-GFP* (+KMD4A-GFP), or *35S:KMD-GFP* (+KMD-GFP) plasmids. Western blots were incubated with anti-GFP (α-GFP) and anti-RFP (α-RFP) antibodies. A higher exposure is shown on the *Bottom* for each antibody. The input and immunoprecipitated (IP α-GFP) fractions were analyzed.

the oryzalin-treated plants remained in many cases associated with the RFP-VPS51 signal (Fig. 5*L*). These results suggest that EMACs occupy stable landmark locations in the cell and may actually anchor the microtubule filaments.

VPS51 Interacts with the Motor Domain of Kinesins. While analyzing the association of the GARP complex with the cytoskeleton, we made the intriguing observation that while VPS51-GFP and KMD-RFP align tightly, RFP-VPS51 and KMD-GFP colocalized completely. In fact, RFP-VPS51 was no longer found in a beads-on-a-string pattern but actually decorated the microtubule filaments (Fig. 6*A*), resembling the distribution of the KMD-GFP protein expressed alone. This tight association between RFP-VPS51 and KMD-GFP was maintained after microtubule depolymerization with oryzalin (*SI Appendix*, Fig. S19), suggesting a direct interaction between VPS51 and KMD. Indeed, RFP-VPS51 coimmunoprecipitated with KMD-GFP, supporting that the VPS51 subunit interacts with the motor domain of the kinesin NtKIN-7K (Fig. 6*B*). Moreover, KMD-RFP did not coimmunoprecipitate with VPS51-GFP, consistent with the inability of KMD-RFP to redistribute VPS51-GFP in vivo. This suggests that the interaction of VPS51 with the motor domain of kinesins requires a free C-terminal end. To test whether the interaction also occurs with *Arabidopsis* kinesins, we made GFP-fusion constructs of the motor domains of KIN-7K (KMD7K-GFP), the closest *Arabidopsis* homolog of NtKIN-7K, of KIN-5A/RSW7 (KMD5A-GFP), the closest *Arabidopsis* homolog of NtKIN-7K outside of subfamily 7, and of KIN-4A/FRA1 (KMD4A-GFP), a well-studied *Arabidopsis* subfamily 4 kinesin that has been linked to microtubule-dependent vesicular transport during cell elongation, possibly for secretion of noncellulosic cell wall components (65). When we expressed them in *Nicotiana benthamiana*, we observed that KMD7K-GFP and KMD5A-GFP strongly labeled microtubules (*SI Appendix*, Fig. S20). Surprisingly, KMD4A-GFP was mainly cytosolic, although it also labeled microtubules weakly. Moreover, KMD4A-GFP had a lower migration in the gel than expected, with only a very minor fraction running at the expected size (~70 kDa) and a major fraction migrating at the gel void (Fig. 6*D*). Importantly, we observed that RFP-VPS51 completely relocated to microtubules when coexpressed with KMD7K-GFP or KMD5A-GFP, and weakly relocated when coexpressed with KMD4A-GFP (Fig. 6*C*). Consistent with this in vivo repositioning, RFP-VPS51 coimmunoprecipitated with KMD7K-GFP, KMD5A-GFP, and

KMD4A-GFP in vitro (Fig. 6*D*), supporting that VPS51 interacts with *Arabidopsis* kinesins through their motor domains.

Discussion

Mechanistic Insights from the Analysis of *mtv* Mutant Alleles. Several of the *mtv* EMS alleles identified here display phenotypes that are different from those of the corresponding knockout mutant alleles, suggesting that they retain activity. Among them, the hypomorphic alleles of the essential genes *MTV10/VPS3*, *MTV11/VPS15*, and *MTV17/VPS54* will be instrumental to determine the biological roles of the CORVET, PI3K, and GARP complexes in adult plants. The *mtv10-1* hypomorphic allele encodes a VPS3 protein lacking the last 62 aa of the protein. Interestingly, *Saccharomyces* VPS3 interacts with the VPS11 CORVET subunit via the C-terminal end of the protein (66), so it may be that this interaction is weakened by the *mtv10-1* deletion. The *mtv11-1* allele encodes a VPS15 protein that retains the N-terminal kinase domain and most of the C-terminal WD40 domain, but lacks the central helical domain. Mutations affecting VPS15 function in yeast and animals cluster in the protein kinase or the WD40 domains (67), highlighting the key role of those domains for the activity of the protein. Moreover, structural analysis of the yeast VPS15 protein shows that the central domain is folded, bringing together the kinase and the WD-40 domains (68), a proximity that is mirrored in the truncated protein encoded by the *mtv11-1* allele, which would explain its partial functionality. In the *mtv17-1* knockdown allele, there is a deletion of the last 21 aa of the protein, which are partially conserved from plants to animals and may, thus, have functional relevance. Indeed, a missense mutation within this domain destabilizes the mouse VPS54 protein, disrupting the GARP complex and causing the wobbler neurodegenerative disease (69). In addition to these alleles in essential genes, two other *mtv* EMS mutants appear to be hypomorphic. The *VPS51* splice acceptor site mutant *mtv16-1* does not show the defects in leaf venation and leaf morphology observed in the strong mutant allele *unh-1* (42), implying that it is a knockdown allele. The *mtv16-1* allele produces *VPS51* transcripts that utilize an alternative splice acceptor site in exon eighth (*SI Appendix*, Fig. S1), which maintains the reading frame and deletes only 14 aa from the protein sequence, explaining how it retains partial activity. The *VSR1* missense mutant *mtv18-1* does not accumulate 12S globulin precursors, as occurs in null *vsr1* mutants, suggesting that it is also a knockdown allele. The P259S mutation in *mtv18-1* lies in the central domain of VSR1, which contributes to ligand binding (70). Hence, this missense mutation may lower the binding affinity for cargo. This reduced affinity could result in secretion of the synthetic VAC2 cargo in aerial tissues, where *VSR1* is moderately expressed, but not of endogenous cargo in seeds, where *VSR1* is expressed at maximal levels (34). In addition to these knockdown alleles, there are others that behave as dominant-negative alleles. The accumulation of 12S globulin precursors in seeds of the *VSR4* mutant *mtv2-3* suggests that this allele interferes dominantly with the redundant *VSR1* and *VSR3* genes (34). The Q222* *mtv2-3* allele codes for a truncated VSR4 protein containing the entire protease-associated (PA) domain involved in cargo binding but lacking the transmembrane and cytosolic domains. Importantly, it has been shown that expression of the luminal ligand binding region of VSRs in *Arabidopsis* interferes dominantly with vacuolar trafficking (46), explaining the dominant-negative function of the *mtv2-3* allele. Similarly, the VAC2 secretion phenotype of the *PTEN2A* mutants *mtv3-1* and *mtv3-6* is recapitulated only when both *PTEN2A* and *PTEN2B* are knocked out, indicating that the *mtv3-1* and *mtv3-6* mutations dominantly interfere with *PTEN2B*. In this regard, it has been shown that, due to dimerization, inactive human PTEN mutant proteins have a dominant-negative effect that is not present in null alleles (71). Hence, heterodimerization of the EMS alleles with PTEN2B probably underlies their dominant-negative effect.

On the Localization of the GARP Retrograde Tethering Complex and the Role of Microtubules and Kinesins in Vacuolar Trafficking. In yeast and animals, the GARP complex is located at the TGN where it tethers endosome-derived retromer vesicles for retrieving, among other proteins, VSRs (19–22). There is evidence that retromer vesicles are also involved in VSR recycling in plants (27), so determining the localization of the GARP complex could reveal the compartment that retrieves VSRs, an unsettled and controversial matter. The two prevailing models propose that it is either the TGN or the ER/Golgi that retrieve VSRs in plants (15, 16, 72). In mammalian cells, retromer vesicles are guided along microtubules to the stationary perinuclear TGN (25). In plants, the ER, Golgi, and TGN are dispersed throughout the cell and are highly dynamic, so it is difficult to envision how retromer vesicles would target those moving organelles, more so when a role for the cytoskeleton in this retrograde transport step in plants had not been reported. Now our results show that the GARP tethering complex is present in EMACs, separate from MVB, TGN, and Golgi markers. EMACs have features that are consistent with being a target organelle for retromer-dependent recycling of VSRs. Their proximity to the ER implies that they may receive anterograde cargo from the ER, which could then be bound by the recycled VSRs for sorting toward the vacuole. Moreover, their association with microtubules and their stability provides a plausible targeting mechanism for the incoming retromer vesicles. In this regard, there is evidence that plant retromer vesicles may associate with microtubules via interaction of SNX1 with CLASP (73). It follows then that microtubules could guide the retromer carriers to EMACs, where they would be tethered by the GARP complex. In addition to this tethering activity, our results suggest that the GARP complex may actually control the dynamics of the incoming vesicles through the interaction between VPS51 and the motor domain of kinesins, a very appealing hypothesis to explore in the future. These findings challenge the assumed notion that, other than in secretion, microtubules have little involvement in vesicle and organelle movement in plants (28). In this challenge, our work joins other recent reports suggesting a role for microtubules in TGN biogenesis and tracking (74) and in trafficking between the MVB and the vacuole (75).

Methods

Plant Materials and Growth Conditions. The EMS-mutagenized population is in the Ler background and was described previously (34). The T-DNA insertion lines *mtv2-2* (*vsr4-2* Salk_094467), *mtv3-2* (*pten2a-2* Salk_114721), *pten2b-1* (Salkseq_120020), *mtv7-2* (*erel1-2* Salk_114362), *mtv8-2* (*arfc1-2* Salk_027975), *mtv9-2* (*puf2-2* Sail_24_C10), *mtv10-2* (*vps3-2* Salk_095163), *mtv10-3* (*vps3-3* Sail_826_A03), *mtv10-4* (*vps3-4* Salk_012514), *mtv11-2* (*vps15-2* Salk_004719), *mtv12-2* (*grv2-9* Salk_067162), *mtv14-3* (*gfs10-2* Salk_139226), *mtv15-2* (*bet11-2* Sail_501_C09), *mtv16-3* (*vps51-3* GK_520G08), and *mtv17-2* (*vps54-3* Salk_08006) are in the Col-0 background and were obtained from the *Arabidopsis* Stock Center. The previously described *mtv18-3/vsr1-1* T-DNA mutant (13) is in the Ws background. *Arabidopsis thaliana* and *Nicotiana benthamiana* plants were grown in a soil/vermiculite mixture (3:1) in the greenhouse under natural light, supplemented with Osram HQL 400-W sodium lamps when illuminance fell below 5,000 lx, and a 16-h light/8-h dark cycle at a temperature range between 22 °C maximum/18 °C minimum. For in vitro culture, plants were grown at 22 °C under 6,000 lux of illuminance in a 16-h light/8-h dark cycle.

Constructs. The *PTEN2A*, *ARFC1*, *PUF2*, *VPS3*, *VPS15*, *GFS10*, *BET11*, *VPS51*, *VPS54*, *CYSP*, and *AtAleurain* cDNAs and the *PTEN2A* and *pten2aG167R* genomic fragments, including 1.5-kb promoter sequence, were PCR amplified using primers listed in *SI Appendix*, Table S1 with Phusion High-Fidelity Polymerase (Thermo Fisher Scientific), cloned into pDONR207 vector for Gateway recombination-based subcloning (Invitrogen), and sequenced verified. The following destination vectors were used: pUBN-Dest and pUBC-Dest (49) for expression in *Nicotiana benthamiana* of fluorescently tagged

proteins under the control of the *ubiquitin-10* promoter; pGWB4 (76) for expression of MTV3 and mtv3-1 fused to GFP under its native promoter, and pPZP, pGWB5, and pGWB6 (76) for expression of fluorescently tagged proteins under the control of the 35S promoter. The compartment markers used were previously described: YFP-MEMB12, YFP-VTI12, YFP-ARA7, RFP-MEMB12, and RFP-ARA7 (77); STtmd-Cherry (78); RFP-SYP61 (79); VHA-a1-RFP (80); GFP-NET3C, NET3B-GFP, VAP27-YFP (62, 63); GFP-MAP4 (81); KMD-RFP (82); GFP-Lifeact (83); RFP-AFVY (47); and STtmd-GFP (84).

Detailed methods can be found in *SI Appendix*.

Data Availability Statement. This article does not contain datasets, code, or materials in addition to those included.

ACKNOWLEDGMENTS. We thank Yolanda Fernández Morón and the Electron Microscopy and the Bioinformatics facilities at the Centro Nacional de Biotecnología–Consejo Superior de Investigaciones Científicas for technical assistance. This work was supported by the Spanish Ministry of Economy and Competitivity and European Regional Development Fund (FEDER) funds (BIO2018-094257-B Ministerio de Ciencia e Innovación/FEDER to E.R., M. Sanmartín, and J.J.S.-S.) and by the Ministry of Education, Youth and Sports of the Czech Republic (LQ1601/CEITEC 2020 grant to J.Z.). G.R. and A.L. were recipients of Formación de Personal Investigador scholarships from the Spanish Ministry of Economy and Competitivity. We thank Dr. Niko Gelner, Dr. Takashi Ueda, Dr. Daniel Van Damme, Dr. Lorenzo Frigerio, Dr. Karin Schumacher, and Dr. Vicente Pallas for kindly providing compartment markers.

1. C. Löfke, K. Dünser, D. Scheuring, J. Kleine-Vehn, Auxin regulates SNARE-dependent vacuolar morphology restricting cell size. *eLife* **4**, e05868 (2015).
2. F. Brandizzi, Transport from the endoplasmic reticulum to the Golgi in plants: Where are we now? *Semin. Cell Dev. Biol.* **80**, 94–105 (2018).
3. S. Wolfenstetter, P. Wirsching, D. Dotzauer, S. Schneider, N. Sauer, Routes to the tonoplast: The sorting of tonoplast transporters in *Arabidopsis* mesophyll protoplasts. *Plant Cell* **24**, 215–232 (2012).
4. Y.-D. Stierhof, C. Viotti, D. Scheuring, S. Sturm, D. G. Robinson, Sorting nexins 1 and 2a locate mainly to the TGN. *Protoplasma* **250**, 235–240 (2013).
5. K. Ebine *et al*., Plant vacuolar trafficking occurs through distinctly regulated pathways. *Curr. Biol.* **24**, 1375–1382 (2014).
6. Q.-N. Feng, Y. Zhang, S. Li, Tonoplast targeting of VHA-a3 relies on a Rab5-mediated but Rab7-independent vacuolar trafficking route. *J. Integr. Plant Biol.* **59**, 230–233 (2017).
7. K. Matsuoka, D. C. Bassham, N. V. Raikhel, K. Nakamura, Different sensitivity to wortmannin of two vacuolar sorting signals indicates the presence of distinct sorting machineries in tobacco cells. *J. Cell Biol.* **130**, 1307–1318 (1995).
8. S. U. Ahmed *et al*., The plant vacuolar sorting receptor AtELP is involved in transport of NH_2-terminal propeptide-containing vacuolar proteins in *Arabidopsis thaliana*. *J. Cell Biol.* **149**, 1335–1344 (2000).
9. E. Stigliano *et al*., Two glycosylated vacuolar GFPs are new markers for ER-to-vacuole sorting. *Plant Physiol. Biochem.* **73**, 337–343 (2013).
10. F. Bottanelli, O. Foresti, S. Hanton, J. Denecke, Vacuolar transport in tobacco leaf epidermis cells involves a single route for soluble cargo and multiple routes for membrane cargo. *Plant Cell* **23**, 3007–3025 (2011).
11. N. Paris *et al*., Molecular cloning and further characterization of a probable plant vacuolar sorting receptor. *Plant Physiol.* **115**, 29–39 (1997).
12. A. A. Sanderfoot *et al*., A putative vacuolar cargo receptor partially colocalizes with AtPEP12p on a prevacuolar compartment in *Arabidopsis* roots. *Proc. Natl. Acad. Sci. U.S.A.* **95**, 9920–9925 (1998).
13. T. Shimada *et al*., Vacuolar sorting receptor for seed storage proteins in *Arabidopsis thaliana*. *Proc. Natl. Acad. Sci. U.S.A.* **100**, 16095–16100 (2003).
14. Y. Lee *et al*., Functional identification of sorting receptors involved in trafficking of soluble lytic vacuolar proteins in vegetative cells of *Arabidopsis*. *Plant Physiol.* **161**, 121–133 (2013).
15. H. Kang, I. Hwang, Vacuolar sorting receptor-mediated trafficking of soluble vacuolar proteins in plant cells. *Plants (Basel)* **3**, 392–408 (2014).
16. G. P. Di Sansebastiano, F. Barozzi, G. Piro, J. Denecke, C. de Marcos Lousa, Trafficking routes to the plant vacuole: Connecting alternative and classical pathways. *J. Exp. Bot.* **69**, 79–90 (2017).
17. M. N. J. Seaman, Retromer and the cation-independent mannose 6-phosphate receptor—time for a trial separation? *Traffic* **19**, 150–152 (2018).
18. K. E. Chen, M. D. Healy, B. M. Collins, Towards a molecular understanding of endosomal trafficking by Retromer and Retriever. *Traffic* **20**, 465–478 (2019).
19. E. Conibear, T. H. Stevens, Vps52p, Vps53p, and Vps54p form a novel multisubunit complex required for protein sorting at the yeast late Golgi. *Mol. Biol. Cell* **11**, 305–323 (2000).
20. F. J. Pérez-Victoria, G. A. Mardones, J. S. Bonifacino, Requirement of the human GARP complex for mannose 6-phosphate-receptor-dependent sorting of cathepsin D to lysosomes. *Mol. Biol. Cell* **19**, 2350–2362 (2008).
21. F. J. Pérez-Victoria *et al*., Ang2/fat-free is a conserved subunit of the Golgi-associated retrograde protein complex. *Mol. Biol. Cell* **21**, 3386–3395 (2010).
22. J. Wei *et al*., The GARP complex is involved in intracellular cholesterol transport via targeting NPC2 to lysosomes. *Cell Rep.* **19**, 2823–2835 (2017).
23. M. Wong, S. Munro, Membrane trafficking. The specificity of vesicle traffic to the Golgi is encoded in the golgin coiled-coil proteins. *Science* **346**, 1256898 (2014).
24. Y. Cui *et al*., Retromer has a selective function in cargo sorting via endosome transport carriers. *J. Cell Biol.* **218**, 615–631 (2019).
25. M. N. J. Seaman, The retromer complex—endosomal protein recycling and beyond. *J. Cell Sci.* **125**, 4693–4702 (2012).
26. T. Wassmer *et al*., The retromer coat complex coordinates endosomal sorting and dynein-mediated transport, with carrier recognition by the *trans*-Golgi network. *Dev. Cell* **17**, 110–122 (2009).
27. P. Oliviusson *et al*., Plant retromer, localized to the prevacuolar compartment and microvesicles in *Arabidopsis*, may interact with vacuolar sorting receptors. *Plant Cell* **18**, 1239–1252 (2006).
28. F. Brandizzi, G. O. Wasteneys, Cytoskeleton-dependent endomembrane organization in plant cells: An emerging role for microtubules. *Plant J.* **75**, 339–349 (2013).
29. A. Nebenführ, R. Dixit, Kinesins and myosins: Molecular motors that coordinate cellular functions in plants. *Annu. Rev. Plant Biol.* **69**, 329–361 (2018).
30. E. Rojo, V. K. Sharma, V. Kovaleva, N. V. Raikhel, J. C. Fletcher, CLV3 is localized to the extracellular space, where it activates the *Arabidopsis* CLAVATA stem cell signaling pathway. *Plant Cell* **14**, 969–977 (2002).
31. M. Sanmartín *et al*., Divergent functions of VTI12 and VTI11 in trafficking to storage and lytic vacuoles in *Arabidopsis*. *Proc. Natl. Acad. Sci. U.S.A.* **104**, 3645–3650 (2007).
32. E. J. Sohn *et al*., The shoot meristem identity gene TFL1 is involved in flower development and trafficking to the protein storage vacuole. *Proc. Natl. Acad. Sci. U.S.A.* **104**, 18801–18806 (2007).
33. J. Zouhar, E. Rojo, D. C. Bassham, AtVPS45 is a positive regulator of the SYP41/SYP61/VTI12 SNARE complex involved in trafficking of vacuolar cargo. *Plant Physiol.* **149**, 1668–1678 (2009).
34. J. Zouhar, A. Muñoz, E. Rojo, Functional specialization within the vacuolar sorting receptor family: VSR1, VSR3 and VSR4 sort vacuolar storage cargo in seeds and vegetative tissues. *Plant J.* **64**, 577–588 (2010).
35. M. Sauer *et al*., MTV1 and MTV4 encode plant-specific ENTH and ARF GAP proteins that mediate clathrin-dependent trafficking of vacuolar cargo from the *trans*-Golgi network. *Plant Cell* **25**, 2217–2235 (2013).
36. I. N. Smith, J. M. Briggs, Structural mutation analysis of PTEN and its genotype-phenotype correlations in endometriosis and cancer. *Proteins* **84**, 1625–1643 (2016).
37. E. Ito *et al*., Integration of two RAB5 groups during endosomal transport in plants. *eLife* **7**, e34064 (2018).
38. N. Xu *et al*., *Arabidopsis* AtVPS15 is essential for pollen development and germination through modulating phosphatidylinositol 3-phosphate formation. *Plant Mol. Biol.* **77**, 251–260 (2011).
39. K. Fuji *et al*., *Arabidopsis* vacuolar sorting mutants (green fluorescent seed) can be identified efficiently by secretion of vacuole-targeted green fluorescent protein in their seeds. *Plant Cell* **19**, 597–609 (2007).
40. K. Tamura *et al*., *Arabidopsis* KAM2/GRV2 is required for proper endosome formation and functions in vacuolar sorting and determination of the embryo growth axis. *Plant Cell* **19**, 320–332 (2007).
41. R. A. Silady *et al*., The GRV2/RME-8 protein of *Arabidopsis* functions in the late endocytic pathway and is required for vacuolar membrane flow. *Plant J.* **53**, 29–41 (2008).
42. S. Pahari *et al*., *Arabidopsis* UNHINGED encodes a VPS51 homolog and reveals a role for the GARP complex in leaf shape and vein patterning. *Development* **141**, 1894–1905 (2014).
43. H. T. Sakurai, T. Inoue, A. Nakano, T. Ueda, ENDOSOMAL RAB EFFECTOR WITH PX-DOMAIN, an interacting partner of RAB5 GTPases, regulates membrane trafficking to protein storage vacuoles in *Arabidopsis*. *Plant Cell* **28**, 1490–1503 (2016).
44. K. Takemoto *et al*., Distinct sets of tethering complexes, SNARE complexes, and Rab GTPases mediate membrane fusion at the vacuole in *Arabidopsis*. *Proc. Natl. Acad. Sci. U.S.A.* **115**, E2457–E2466 (2018).
45. M. S. Otegui, R. Herder, J. Schulze, R. Jung, L. A. Staehelin, The proteolytic processing of seed storage proteins in *Arabidopsis* embryo cells starts in the multivesicular bodies. *Plant Cell* **18**, 2567–2581 (2006).
46. J. Shen *et al*., An in vivo expression system for the identification of cargo proteins of vacuolar sorting receptors in *Arabidopsis* culture cells. *Plant J.* **75**, 1003–1017 (2013).
47. P. R. Hunter, C. P. Craddock, S. Di Benedetto, L. M. Roberts, L. Frigerio, Fluorescent reporter proteins for the tonoplast and the vacuolar lumen identify a single vacuolar compartment in *Arabidopsis* cells. *Plant Physiol.* **145**, 1371–1382 (2007).
48. Y. C. Tse *et al*., Identification of multivesicular bodies as prevacuolar compartments in *Nicotiana tabacum* BY-2 cells. *Plant Cell* **16**, 672–693 (2004).
49. C. Grefen *et al*., A ubiquitin-10 promoter-based vector set for fluorescent protein tagging facilitates temporal stability and native protein distribution in transient and stable expression studies. *Plant J.* **64**, 355–365 (2010).
50. C. Rosa-Ferreira, C. Christis, I. L. Torres, S. Munro, The small G protein Arl5 contributes to endosome-to-Golgi traffic by aiding the recruitment of the GARP complex to the Golgi. *Biol. Open* **4**, 474–481 (2015).
51. S. E. Murthy *et al*., OSCA/TMEM63 are an evolutionarily conserved family of mechanically activated ion channels. *eLife* **7**, e41844 (2018).
52. F. Yuan *et al*., OSCA1 mediates osmotic-stress-evoked Ca^{2+} increases vital for osmosensing in *Arabidopsis*. *Nature* **514**, 367–371 (2014).
53. K. Maity *et al*., Cryo-EM structure of OSCA1.2 from *Oryza sativa* elucidates the mechanical basis of potential membrane hyperosmolality gating. *Proc. Natl. Acad. Sci. U.S.A.* **116**, 14309–14318 (2019).
54. T. Zhang *et al*., The mammalian protein (rbet1) homologous to yeast Bet1p is primarily associated with the pre-Golgi intermediate compartment and is involved in vesicular transport from the endoplasmic reticulum to the Golgi apparatus. *J. Cell Biol.* **139**, 1157–1168 (1997).

55. J. Malsam, T. H. Söllner, Organization of SNAREs within the Golgi stack. *Cold Spring Harb. Perspect. Biol.* **3**, a005249 (2011).
56. T. Uemura *et al*., Systematic analysis of SNARE molecules in *Arabidopsis*: Dissection of the post-Golgi network in plant cells. *Cell Struct. Funct.* **29**, 49–65 (2004).
57. L. C. Wang *et al*., Involvement of the *Arabidopsis* HIT1/AtVPS53 tethering protein homologue in the acclimation of the plasma membrane to heat stress. *J. Exp. Bot.* **62**, 3609–3620 (2011).
58. E. Lobstein *et al*., The putative *Arabidopsis* homolog of yeast vps52p is required for pollen tube elongation, localizes to Golgi, and might be involved in vesicle trafficking. *Plant Physiol.* **135**, 1480–1490 (2004).
59. H. Guermonprez *et al*., The POK/AtVPS52 protein localizes to several distinct post-Golgi compartments in sporophytic and gametophytic cells. *J. Exp. Bot.* **59**, 3087–3098 (2008).
60. T. J. Hawkins, M. J. Deeks, P. Wang, P. J. Hussey, The evolution of the actin binding NET superfamily. *Front Plant Sci* **5**, 254 (2014).
61. M. J. Deeks *et al*., A superfamily of actin-binding proteins at the actin-membrane nexus of higher plants. *Curr. Biol.* **22**, 1595–1600 (2012).
62. P. Wang *et al*., The plant cytoskeleton, NET3C, and VAP27 mediate the link between the plasma membrane and endoplasmic reticulum. *Curr. Biol.* **24**, 1397–1405 (2014).
63. P. Wang, P. J. Hussey, NETWORKED 3B: A novel protein in the actin cytoskeleton-endoplasmic reticulum interaction. *J. Exp. Bot.* **68**, 1441–1450 (2017).
64. T. Hamada *et al*., RNA processing bodies, peroxisomes, Golgi bodies, mitochondria, and endoplasmic reticulum tubule junctions frequently pause at cortical microtubules. *Plant Cell Physiol.* **53**, 699–708 (2012).
65. Z. Kong *et al*., Kinesin-4 functions in vesicular transport on cortical microtubules and regulates cell wall mechanics during cell elongation in plants. *Mol. Plant* **8**, 1011–1023 (2015).
66. R. L. Plemel *et al*., Subunit organization and Rab interactions of Vps-C protein complexes that control endolysosomal membrane traffic. *Mol. Biol. Cell* **22**, 1353–1363 (2011).
67. Y. Ohashi, S. Tremel, R. L. Williams, VPS34 complexes from a structural perspective. *J. Lipid Res.* **60**, 229–241 (2019).
68. K. Rostislavleva *et al*., Structure and flexibility of the endosomal Vps34 complex reveals the basis of its function on membranes. *Science* **350**, aac7365 (2015).
69. F. J. Pérez-Victoria *et al*., Structural basis for the wobbler mouse neurodegenerative disorder caused by mutation in the Vps54 subunit of the GARP complex. *Proc. Natl. Acad. Sci. U.S.A.* **107**, 12860–12865 (2010).
70. X. Cao, S. W. Rogers, J. Butler, L. Beevers, J. C. Rogers, Structural requirements for ligand binding by a probable plant vacuolar sorting receptor. *Plant Cell* **12**, 493–506 (2000).
71. A. Papa *et al*., Cancer-associated PTEN mutants act in a dominant-negative manner to suppress PTEN protein function. *Cell* **157**, 595–610 (2014).
72. S. Früholz *et al*., Nanobody-triggered lockdown of VSRs reveals ligand reloading in the Golgi. *Nature Commun.* **9**, 643 (2018).
73. C. Ambrose *et al*., CLASP interacts with sorting nexin 1 to link microtubules and auxin transport via PIN2 recycling in *Arabidopsis thaliana*. *Dev. Cell* **24**, 649–659 (2013).
74. L. Renna *et al*., TGNap1 is required for microtubule-dependent homeostasis of a subpopulation of the plant *trans*-Golgi network. *Nat. Commun.* **9**, 5313 (2018).
75. E. Onelli *et al*., Microtubules play a role in trafficking prevacuolar compartments to vacuoles in tobacco pollen tubes. *Open Biol.* **8**, 180078 (2018).
76. T. Nakagawa *et al*., Improved Gateway binary vectors: High-performance vectors for creation of fusion constructs in transgenic analysis of plants. *Biosci. Biotechnol. Biochem.* **71**, 2095–2100 (2007).
77. N. Geldner *et al*., Rapid, combinatorial analysis of membrane compartments in intact plants with a multicolor marker set. *Plant J.* **59**, 169–178 (2009).
78. M. Serra-Soriano, V. Pallás, J. A. Navarro, A model for transport of a viral membrane protein through the early secretory pathway: Minimal sequence and endoplasmic reticulum lateral mobility requirements. *Plant J.* **77**, 863–879 (2014).
79. S. W. Choi *et al*., RABA members act in distinct steps of subcellular trafficking of the FLAGELLIN SENSING2 receptor. *Plant Cell* **25**, 1174–1187 (2013).
80. J. Dettmer, A. Hong-Hermesdorf, Y. D. Stierhof, K. Schumacher, Vacuolar H^+-ATPase activity is required for endocytic and secretory trafficking in *Arabidopsis*. *Plant Cell* **18**, 715–730 (2006).
81. J. Marc *et al*., A GFP-MAP4 reporter gene for visualizing cortical microtubule rearrangements in living epidermal cells. *Plant Cell* **10**, 1927–1940 (1998).
82. M. J. Deeks *et al*., The plant formin AtFH4 interacts with both actin and microtubules, and contains a newly identified microtubule-binding domain. *J. Cell Sci.* **123**, 1209–1215 (2010).
83. A. P. Smertenko, M. J. Deeks, P. J. Hussey, Strategies of actin reorganisation in plant cells. *J. Cell Sci.* **123**, 3019–3028 (2010).
84. P. Boevink *et al*., Stacks on tracks: The plant Golgi apparatus traffics on an actin/ER network. *Plant J.* **15**, 441–447 (1998).